RSC Advances

PAPER

View Article Online
View Journal | View Issue

Cite this: *RSC Adv.*, 2024, **14**, 30452

Tuning liquid crystal properties with ZnO nanodiscs: a study on order parameter and conductivity

Shweta Mishra, V. Manjuladevi * and R. K. Gupta

Received 31st July 2024
Accepted 18th September 2024

DOI: 10.1039/d4ra05558f

rsc.li/rsc-advances

Anisotropic nanostructures dispersed in nematic liquid crystal, 4-(*trans*-4′-pentylcyclohexyl)-benzonitrile (PCH5), tend to improve the properties of host nematic liquid crystal owing to its structure and strong dipolar interactions. The experimental investigations of such composite systems are intriguing as well as challenging. Here, we have presented a systematic experimental study of effect of incorporation of two-dimensional anisotropic nanostructure, *i.e.*, nanodisc on properties of room temperature nematic liquid crystal. Zinc oxide nanodiscs (ZD) of thickness ~ 50 nm and diameter ~ 200 nm are synthesized using hydrothermal method and characterized. Dispersion of zinc oxide nanodiscs in PCH5 is observed to increase the dielectric anisotropy and elastic constants which indicate enhancement in the order parameter of the composite system as compared to host nematic liquid crystal. Bulk ac conductivity is also observed to be decreasing by ~60% by dispersion of zinc oxide nanodiscs in host liquid crystal. The increase in the ratio of bend to splay elastic constant makes the ZD composites of PCH5 potential candidates for higher multiplexing devices.

1. Introduction

Research on the impact of nanomaterials on the physical properties of liquid crystals (LCs) is gaining significant attention. Among the various LC phases, the nematic phase exhibited by calamitic liquid crystals is particularly valuable for display devices due to its long-range orientational order, low viscosity, and high visco-elastic coefficient. Nematic liquid crystals (NLCs) are not only easy to align but also can be switched using low electric field strengths.[1] Dispersion of variety of nanoparticles such as[2] semiconducting,[3] ferroelectric,[4] magnetic[5] nanoparticles in LC matrix has been investigated.[6,7] Advancement in important display device parameters such as switching time, threshold voltage and bend to splay elastic constant ratio by doping different nanoparticles has been reported by several researchers. Shape anisotropy of dispersed nanoparticles in LC matrix plays a crucial role in modification of physical properties of NLCs.[8,9] It has been observed that addition of anisotropic nanostructures to LCs improve the device parameters to great extent. However, these improvements depend on various factors such as shape, size, and surface to volume ratio of a nanoparticle, concentration of nanoparticles in LC and LC–nanoparticle interactions. Effect of dispersion of anisotropic nanostructures such as nanorods,[10–12] nanowires,[13,14] nanotubes,[15–17] nanoplatelets,[18,19] nanosheets[20,21] in LC on various properties of LCs have been studied by few research groups. Yet, synthesis procedures, control over the crystallinity, phase purity of anisotropic nanoparticles and difficulty in dispersion characteristics of anisotropic nanostructures in LC slowed the progress of the research in this area. The variation of dielectric and electro-optic properties of NLCs with the dispersion of graphene oxide is studied briefly due to its interesting properties.[22–24] However, reports on experimental investigation of dispersion of 2D nanomaterials/nanodiscs in NLC is very scarce. This article aims to understand the influence of 2D nanostructures of controlled dimensions (apart from carbonaceous 2D structures) on dielectric and switching behaviour of NLC. In this article, we have reported the effect of incorporation of zinc oxide nanodiscs on various physical parameters of a NLC. Due to the ability to be applied in various downstream applications, zinc oxide (ZnO) is one of the most widely studied nanomaterial. ZnO is abundant, inexpensive, safe, and can be prepared easily. ZnO nanomaterials show tunable physical and chemical behaviours as a function of shape of a nanoparticle. With the energy band of 3.37 eV and a bonding energy of 60 meV, ZnO nanomaterials exhibit excellent chemical, electrical, and thermal stabilities along with optical, electrical, and photocatalytic properties. Hence, ZnO nanomaterials find widespread applications in the field of solar cells, photocatalysis, chemical sensor, biological labelling, biological sensing, multifunctional nanocarriers for drug delivery, gene delivery, nanomedicine as well as ceramics.[25,26] Here, we have synthesized disc shaped nanoparticles of ZnO using hydrothermal method. Further, temperature dependent variations of essential physical properties of NLC such as dielectric permittivity, elastic

Department of Physics, Birla Institute of Technology & Science (BITS Pilani), Pilani, Rajasthan, India, 333031. E-mail: manjula@pilani.bits-pilani.ac.in

constants and electro-optic switching with the dispersion of different concentrations of ZnO nanodisc in NLC is reported.

2. Experimental

2.1. Materials

4-(*trans*-4′-Pentylcyclohexyl)-benzonitrile (PCH5) and zinc acetate dihydrate ($Zn(ac)_2 \cdot 2H_2O$) are procured from Sigma-Aldrich. Sodium hydroxide (NaOH) and Ethanol are procured from Merck, Milli-Q water (Merck Milli-Q DQ-3).

2.2. Synthesis of ZnO nanodisc

Zinc oxide nanodiscs (ZDs) are synthesized using a hydrothermal method. Separate 0.1 M solutions of zinc acetate dihydrate [$Zn(ac)_2 \cdot 2H_2O$] and 0.5 M sodium hydroxide (NaOH) were prepared with Milli-Q water as the solvent. These solutions were mixed and stirred vigorously until a clear, transparent solution was achieved. This solution was then transferred to a 100 mL steel autoclave with a Teflon liner. The autoclave was maintained at 150 °C for approximately 24 hours and allowed to cool naturally to room temperature. The resulting precipitate was separated by centrifugation and washed three times with ethanol. The final product was dried in air at 60 °C for 2 hours. The powdered sample was then preserved for further characterization and preparation of liquid crystal composites.

2.3. Preparation of composite sample

For the experimental study, host NLC, 4-(*trans*-4′-pentylcyclohexyl)-benzonitrile (PCH5) which exhibits a phase transition sequence of isotropic (55.3 °C) nematic (30 °C) crystal procured from Sigma-Aldrich is used without further purification.

Composites were prepared using the synthesized zinc oxide nanodiscs (ZDs). The ZDs were dissolved in chloroform and subjected to ultrasonication for approximately two hours to achieve homogeneous dispersions. Specific amounts of these dispersions were then added to the host nematic liquid crystal (NLC) to achieve ZD concentrations (C_{ZD}) of 0.01, 0.02, 0.05, and 0.1 weight percent (wt%). The composite solutions were further sonicated to ensure uniform mixing and then allowed to stand until the solvent had completely evaporated.

2.4. Characterization techniques

2.4.1. Characterization of nanomaterials. The crystalline phase of the synthesized zinc oxide nanodisc (ZD) powder was determined using powder X-ray diffraction (XRD). The analysis was conducted with a Rigaku SmartLab Studio X-ray diffractometer, utilizing Cu Kα radiation (λ = 1.5406 Å). The scans were performed in the 2θ range of 10° to 90° at a scanning rate of 4° per minute, with the instrument operating at a voltage of 40 kV. The morphology of the synthesized particles was examined using a field emission scanning electron microscope (FE-SEM; FEI Apreo LoVac).

2.4.2. Characterization of pure NLC and its composites. For the electro-optic and dielectric measurements, planar-aligned cells with a thickness of approximately 7 μm and an area of around 0.8 cm^2 were fabricated. The process began by spin-coating a layer of polyimide (PI2555) onto indium tin oxide (ITO)-coated glass plates, followed by curing at 250 °C for about an hour. After curing, the PI-coated substrates were unidirectionally rubbed with a soft cloth and placed with the rubbing directions antiparallel to each other. These plates were then assembled using epoxy glue mixed with glass spacers to form a final planar-aligned sandwich cell. The thickness of the fabricated planar-aligned sample cells was measured using an interferometry-based fiber-optic spectrometer (Ocean Optics USB4000-XR1-ES). The dispersion properties of the zinc oxide nanodiscs (ZD) in a nematic matrix within the cell were examined using fluorescence confocal microscopy (LSM880, Zeiss). Optical texture studies of the sample cells, filled with both pure and composite samples of nematic liquid crystals (NLC), were conducted using a polarizing optical microscope (POM; Olympus BX53M). The sample cell was placed inside a temperature-controlled hot stage (Micro-Optik MDTC600) with a resolution of 0.1 °C, which featured a small hole to allow light to pass through. The hot stage containing the sample cell was positioned on the rotating stage of the POM between crossed polarizers. A laser beam with a wavelength of 633 nm was directed through the sample, and the planar-aligned cell was adjusted between the crossed polarizers so that the rubbing direction was at a 45° angle to either polarizer. The transmitted intensity (I) as a function of temperature was recorded and used to estimate the birefringence (Δn) of the nematic samples according to the equation

$$I = I_0 \sin^2\left(\frac{\pi d\langle \Delta n\rangle}{\lambda}\right)$$

where I is the transmitted intensity from the analyser, I_0 is the intensity of the plane-polarized light incident on the LC cell, d is the cell thickness, and λ is the wavelength of the monochromatic light.

The measurement of electro-optic switching times, including rise time (τ_r), decay time (τ_d) and total response time ($\tau_R = \tau_r + \tau_d$), for both pure and composites of NLC was conducted using a digital storage oscilloscope (DSO; Keysight EDUX1002G). A square wave with a frequency of 60 Hz was applied at various voltages. Additionally, various dielectric parameters such as dielectric permittivity (ε), dielectric anisotropy ($\Delta\varepsilon$), threshold voltage (V_{th}) and bulk ac conductivity (σ_{ac}) were measured following previously reported method.[13]

3. Results and discussion

The synthesized nanomaterials are characterized for phase purity and morphological investigations. XRD analysis was performed to study the structural properties of as synthesized ZD as shown in Fig. 1a. All the peaks are identified and the corresponding miller indices are evaluated which are marked on the XRD graph in Fig. 1a. All the peaks observed in Fig. 1a correspond closely to those of standard bulk ZnO, which is known to exhibit a hexagonal wurtzite crystal structure ($P6_3mc$, JCPDF no. 36-1451). The presence of distinct sharp peaks in XRD diffraction pattern indicates formation of highly pure ZnO

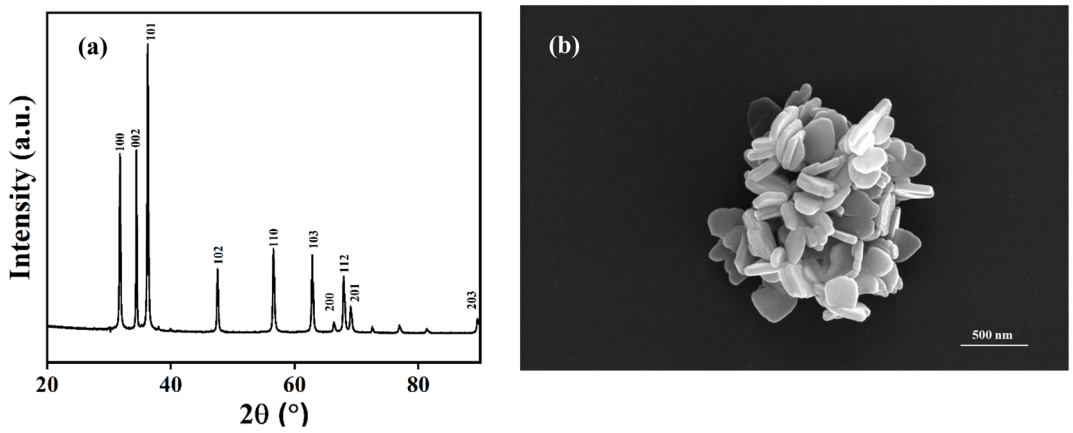

Fig. 1 (a) Powder X-ray diffraction pattern; (b) FESEM image of as synthesized zinc oxide nanodiscs.

nanoparticles. Morphological investigation of ZD using the FE-SEM is shown in Fig. 1b. Formation of nanodiscs is clearly visible from the recorded images. The average thickness and diameter of ZnO nanodiscs was measured and found to be ~50 nm and ~200 nm, respectively.

Dispersion of ZD in NLC matrix is examined using fluorescent confocal microscopy (FCM). The recorded images are shown in Fig. 2. As the ZnO nanoparticles are fluorescent under UV emission, we can observe the emission from nanoparticles distributed in NLC matrix when illuminated under UV laser of wavelength $\lambda \sim 370$ nm. The blue spots observed in Fig. 2 shows the emission from ZnO nanodiscs dispersed in NLC matrix. However, no emission is observed in recorded FCM images of pure NLC sample.

Moreover, it has been observed that at $C_{ZD} \leq 0.05$, nanodiscs are uniformly dispersed in the bulk of NLC matrix. However, at C_{ZD} =0.1, nanodiscs are observed to be preferentially near the substrate surfaces of the cell as compared to that in the bulk of the NLC matrix. Nonetheless, we can observe uniform dispersion of ZD in NLC matrix.

The optical textures of pure NLC and composite samples filled in planar aligned cells are observed under crossed polarizers of POM and the recorded images are shown in Fig. 3. In Fig. 3, first row showing bright images are recorded when sample alignment is at 45° between crossed polarizers and second row depicting dark images are recorded when sample alignment is parallel to either of the crossed polarizers. The uniform colours of the images depict homogeneous alignment of pure NLC molecules. The uniform optical textures are maintained even after dispersion of ZD in PCH5. It can be inferred that addition of ZD with the specified concentration in PCH5 form the homogeneous composites with uniformly distributed ZD in nematic matrix. However, the aggregation of nanodiscs can be observed in POM image of nanocomposite sample with $C_{ZD} = 0.1$. Although, no changes in the planar alignment of NLC molecules is observed with the dispersion of ZD for the composites under investigation.

Variation of birefringence (Δn) of pure and ZD composites of PCH5 with varying temperature is shown in Fig. 4. Inset of Fig. 4 shows the variation of Δn as a function of C_{ZD} in PCH5 at $T - T_{IN} = -15$ °C. The birefringence of PCH5 increases with the

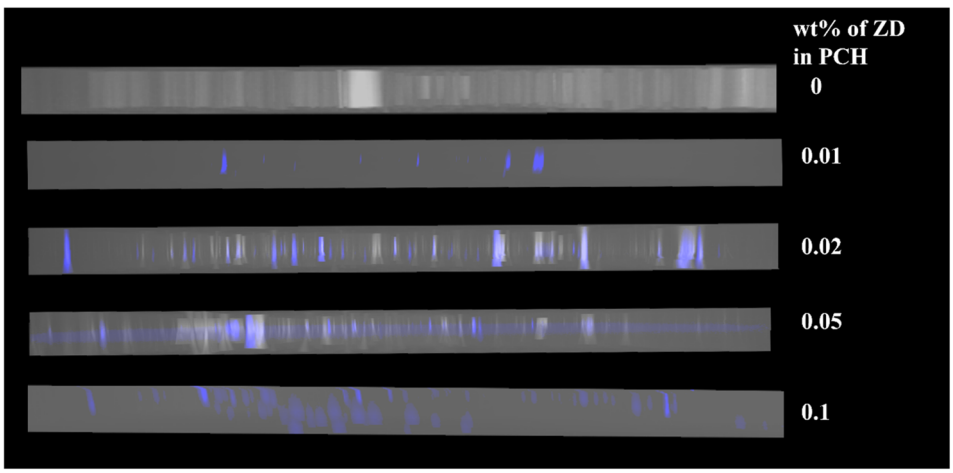

Fig. 2 Fluorescence confocal microscopy images of pure and ZnO nanodisc incorporated PCH5.

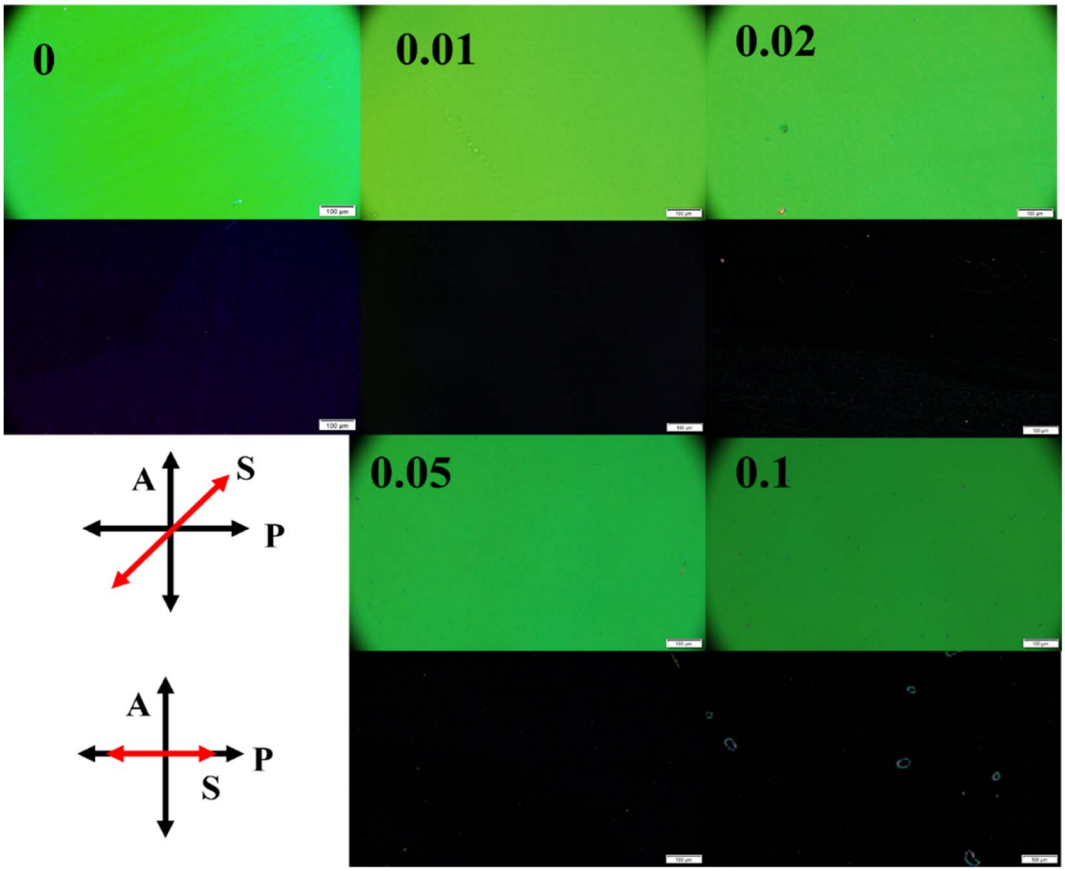

Fig. 3 The optical textures of both pure and ZD-dispersed PCH5, filled in planar cells, were visualized using crossed polarizers in a polarizing optical microscope (POM); numbers indicate C_{ZD}. (A: analyser, P: polarizer, S: sample cell; arrow indicate the alignment direction); scale: 100 μm; all images are recorded at $T = 35$ °C.

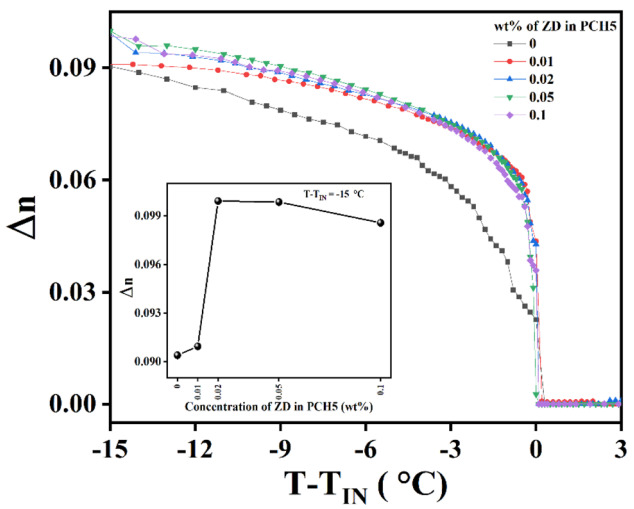

Fig. 4 Variation of birefringence (Δn) of pure and ZD dispersed PCH5 as a function of temperature; (inset shows variation of Δn as a function of concentration of ZD in PCH5 at $T - T_{IN} = -15$ °C).

addition of ZD and shows a monotonic behaviour. However, with the aggregation of ZD, values of Δn starts decreasing but are still greater than that of pure of PCH5. Increase in the value of Δn can be due to increase in the order parameter of the composite system as compared to that of pure PCH5. The pseudo-nematic domains near both surfaces of ZD in the composite samples form due to the coherent alignment of NLC molecules through epitaxial interactions. These pseudo-nematic domains exhibit varying anisotropy compared to the bulk LC, influenced by the surface symmetry of the ZD. The LC–ZD domains align their flat planes parallel to the far-field nematic director in the NLC, thereby minimizing the elastic distortion of the nematic phase and reducing the overall free energy. Hence, additional orientational order is acquired due to NLC–ZD interaction which can be visualized as local anchoring fields along the nematic director. The further experimental results of dielectric measurements support these arguments.

Dielectric properties such as dielectric permittivity, dielectric anisotropy, threshold voltage, splay and bend elastic constant of NLC are crucial parameters for device applications. The dielectric properties signify applications of NLCs depending on orientation transition under the application of externally applied electric field. All the mentioned dielectric parameters as a function of temperature for pure and ZD dispersed PCH5 are measured at applied frequency of 4.1 kHz. Fig. 5a shows the variation of perpendicular ($\varepsilon_\perp$) and parallel ($\varepsilon_\parallel$) components of dielectric permittivity with the incorporation of ZD in PCH5.

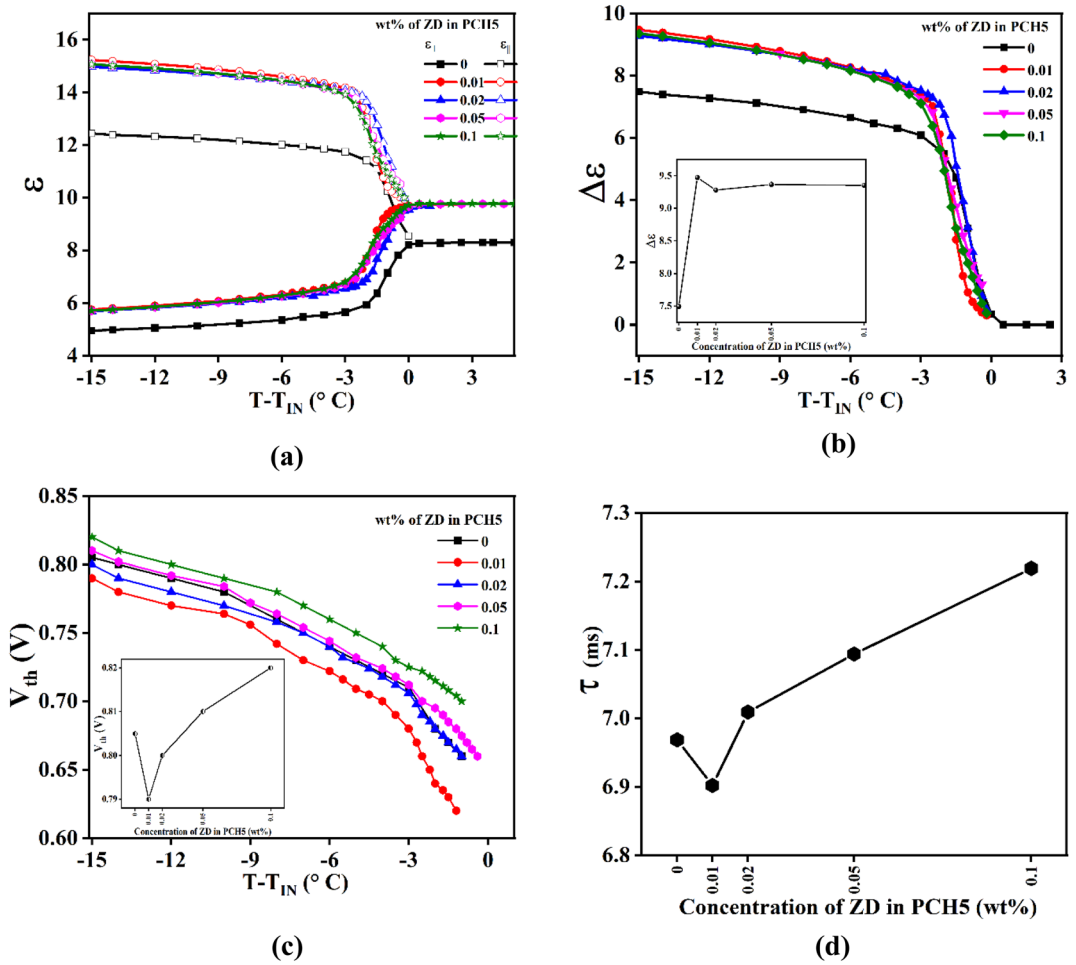

Fig. 5 Temperature variation of (a) perpendicular ($\varepsilon_\perp$) and parallel ($\varepsilon_\parallel$) components of dielectric permittivity (b) dielectric anisotropy ($\Delta\varepsilon$) (inset shows variation of $\Delta\varepsilon$ as a function of C_{ZD} in PCH5) (c) threshold voltage (V_{th}) (inset shows variation of V_{th} as a function of C_{ZD} in PCH5); for pure and ZD dispersed PCH5 measured at applied frequency of 4 kHz (d) electro-optic response time (τ); for pure and ZD dispersed PCH5 measured at applied frequency of 60 Hz.

Both the components increase in ZD composites of PCH5 as compared to that of pure PCH5. But the relative increase in $\varepsilon_\parallel$ is larger than that of $\varepsilon_\perp$ for composites with respect to that of pure PCH5. The variation of dielectric anisotropy ($\Delta\varepsilon = \varepsilon_\parallel - \varepsilon_\perp$) of pure and ZD dispersed PCH5 is shown in Fig. 5b. The value of $\Delta\varepsilon$ increases by ~27% with incorporation of ZD in PCH5. It slightly decreases for $C_{ZD} \geq 0.02$ wt% but is still higher than that of pure PCH5. Similar results have been reported previously.[8,11]

Orlandi *et al.*[9] reported simulation based study of nanodisc dispersed in nematic mesogens. Based on the observed results,[9] they have concluded that disc shaped nanoparticles can accommodate within the ordered structure of the mesogens with host mesogens molecules aligning parallel to their plane as well as to the LC director due to its flat shape. It means disc-like nanoparticles are more likely to align their axis (axis along thickness of disc) perpendicular to the NLC director as shown in the Fig. 6. However, increase in concentration of nanodiscs may lead to formation of dimers or stacking of discs causing aggregation which is expected to destabilize the nematic phase.

The value of $\Delta\varepsilon$ is directly proportional to macroscopic order parameter according to Maier–Meier theory. Whereas, perpendicular ($\varepsilon_\perp$) and parallel ($\varepsilon_\parallel$) components of dielectric permittivity relates to antiparallel and parallel correlation, respectively, amongst the NLC molecules. The reports on experimental investigations of NLC–gold nanocomposite systems by Sridevi *et al.*[27] suggested that increase in the value of $\Delta\varepsilon$ can be due to increase in orientational ordering or decrease in the antiparallel correlation of neighbouring NLC molecules. Based on our experimental results, we can observe that the value of $\Delta\varepsilon$ as well as Δn increases with the incorporation of nanodiscs in PCH5 as compared to pure PCH5. Also, as discussed above, both the components of dielectric permittivity increase with the dispersion of ZD in PCH5 as compared to pure NLC. Therefore, we suggest that NLC molecules align in a plane parallel to the nanodisc surface which may result in achieving higher order parameter with the dispersion of ZD in PCH5 as compared to pure NLC. The thermal energy is not strong enough to eradicate the anchoring mechanisms of LC–ZD at the interfaces in the isotropic phase. Thus, the presence of pseudo

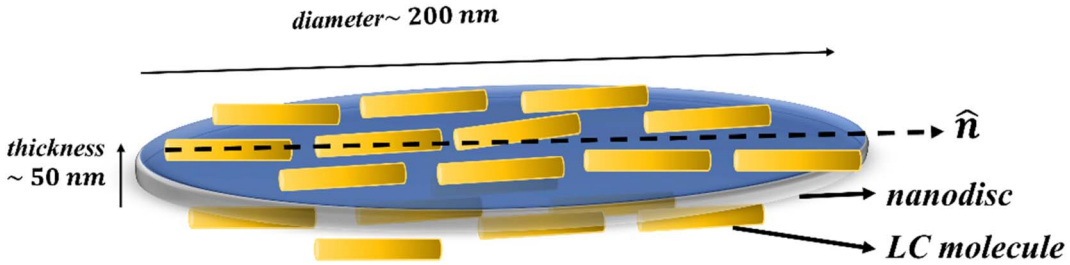

Fig. 6 Schematic showing arrangement of NLC molecules around nanodisc.

nematic domains is also expected in the isotropic phase of the nanocomposite samples. This also explains the experimentally observed increase in the value of ε in the isotropic phase of composites samples as compared to that of pure PCH5.

Freedericksz transition voltage (V_{th}) of pure PCH5 and its ZD composites as a function of temperature is shown in Fig. 5c. The value of V_{th} decreases for $C_{ZD} \leq 0.02$ wt% and then increases with further increase in $C_{ZD} \geq 0.05$ wt% as compared to pure PCH5. However, the decrease in the value of V_{th} is not appreciably large. This may be because of the shape of the nanoparticle. It is likely due to a stronger planar anchoring of the liquid crystal molecules on the surface of the ZnO nanodiscs which remain parallel to the substrate plane with the application of external electric field is applied.[23] With dispersion of nanodiscs, local domains of NLC molecules with director aligned parallel to plane of disc are created (Fig. 6). At lower concentration ($C_{ZD} \leq 0.02$ wt%), these domains being homogeneously distributed across the NLC matrix, are easier to align at low applied voltages. However, with increase in C_{ZD}, formation of aggregates as seen from POM images and FCM images, only allows the switching of NLC molecules at higher applied voltages. Increasing the C_{ZD} leads to an increase in V_{th} until the switching of the liquid crystal molecules is dominated by the domains of LC molecules around dispersed ZnO nanodiscs. Similarly, the electro-optic response time is also observed to be decreasing for $C_{ZD} = 0.01$ wt% as compared to pure PCH5 and then increases with further increase in the C_{ZD} in PCH5. Hence, it may be inferred that incorporation of nanodiscs may slow down the switching behaviour of host NLC molecules.

Elastic constants of the NLC are also one of the parameters to understand the ordering in the system. According to Frank–Oseen theory, all primary elastic constants, K_{ii} (i: splay, bend, and twist) are directly proportional to square of the order parameter. In planar cell geometry, we can only measure the splay (K_{11}) and bend (K_{33}) elastic constants as twist is negligible. Fig. 7a and b illustrate the variations in K_{11} and K_{33} of pure and ZD-dispersed PCH5 as functions of temperature. The observed increase in K_{11} can be attributed to slight changes in molecular structure or interactions that enhance the tendency for molecular alignment along the director axis. This increase in K_{11} may result from factors such as improved molecular packing, stronger intermolecular forces, or greater molecular rigidity.[28,29] On the other hand, the elastic constant K_{33}, which reflects the energy associated with molecular alignment within the plane of the cell substrate, shows that a significant rise in K_{33} indicates a greater inclination for molecular alignment within the substrate plane. The disc shaped nanoparticles help NLC molecules to arrange with the director parallel to disc plane which in turn is parallel to cell substrate. This can be attributed to the observed increase in the value of K_{33} with the incorporation of ZD in PCH5 as compared to pure NLC. The observed increase in the value of K_{11} as well as K_{33} shows the enhanced orientational ordering in the composite system with the dispersion of ZD in PCH5 as compared to pure PCH5. The ratio of K_{33}/K_{11} with varying temperature is shown in Fig. 8a for pure

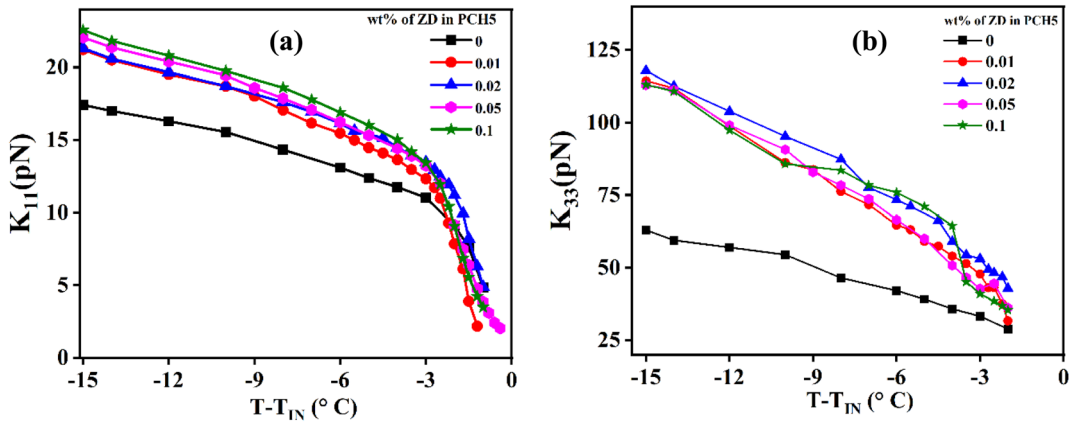

Fig. 7 (a) Splay (K_{11}) and (b) bend (K_{33}) elastic constant as a function of temperature for pure and ZD dispersed PCH5.

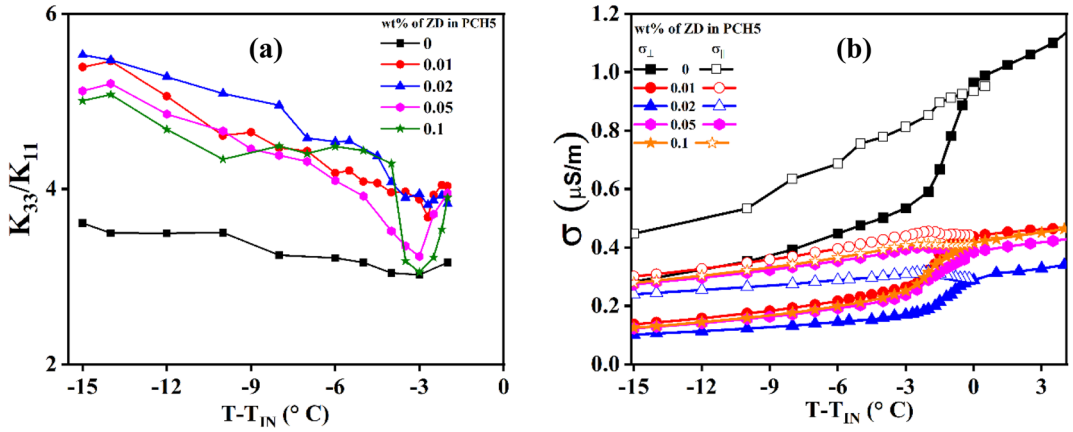

Fig. 8 (a) Ratio of bend (K_{33}) to splay (K_{11}) elastic constant (b) bulk ac conductivity (σ) with varying temperature for pure and ZD dispersed PCH5.

and ZD composites of PCH5. Increase in the molecular ordering and strengthened intermolecular interactions leads to increase in the value of K_{33}/K_{11} of ZD composites of PCH5 as compared to pure NLC which can be potentially used for high multiplexing devices. Reduction of the ionic impurities in host NLC is also one of the important challenges to achieve better quality displays. The bulk ac conductivity (σ) of the pure and ZD composites of PCH5 is measured and plotted as shown in Fig. 8b. The conductivity of composites is found to be reduced by ~60% with the addition of ZD in PCH5 as compared to that of pure PCH5. Decrease in the value of bulk ac conductivity of nanocomposite samples can potentially be attributed to trapping of ionic impurities by dispersed nanodiscs. Zinc oxide nanoparticles are better known for their ion trapping properties when dispersed in NLC.[8,11] The large surface to volume ratio of nanodiscs provides sufficient trapping sites for ionic impurities in the NLC medium.

4. Conclusion

A study on modification in the dielectric and electro-optic properties of nematic liquid crystal with incorporation of two dimensional nanodiscs is carried out. Zinc oxide nanodiscs (ZD) of diameter ~ 200 nm and thickness ~ 50 nm are synthesized using hydrothermal method. X-ray diffraction spectra indicate formation of crystalline zinc oxide nanoparticles with characteristic peaks corresponding to wurtzite hexagonal lattice structure. Morphology of as prepared nanoparticles to be disc shaped is confirmed by field emission scanning electron microscopy. Composites of ZD dispersed in room temperature nematic liquid crystal are prepared at different concentrations, *viz.*, 0.01, 0.02, 0.05 and 0.1 wt% of pure NLC. Increase in the parallel and perpendicular components of dielectric permittivity is observed in ZD composites as compared to pure NLC. The increment in the birefringence, dielectric anisotropy as well as elastic constants (splay and bend) of ZD composites of NLC is observed as compared to pure NLC which clearly indicates the enhancement in orientational order of the NLC host with the incorporation of nanodiscs. The bulk ac conductivity of the nanocomposite samples also decreases by ~60% with the incorporation of ZD in NLC. However, the Freedericksz transition voltage (V_{th}) of composites shows negligible change as compared to pure NLC. Further, the electro-optic response time of the nanocomposite samples remains unaffected at lower concentrations of ZD (0.01 wt%) in PCH5 and goes on increasing with increasing concentration of ZD (>0.01 wt%) in PCH5. Hence, we conclude that incorporation of anisotropic two-dimensional zinc oxide nanodiscs helps in enhancement of orientational order in the nanocomposite system and can be explored as a potential candidate for higher multiplexing devices.

Data availability

The data presented in the article will be made available upon reader's request.

Conflicts of interest

There are no conflicts of interest to declare.

Acknowledgements

The authors SM and MV express their sincere gratitude to DST SERB for their support under project number EMR/2016/005782 and to BITS Pilani. VM also acknowledges SERB for their support under project number SPG/2021/002260. We appreciate the Department of Physics at BITS Pilani, Pilani Campus for granting access to the XRD facility, established with funding from DST-FIST (No. SR/FST/PS-I/2017/30). Additionally, we are thankful to the Department of Chemical Engineering at BITS Pilani, Pilani Campus for providing various experimental facilities.

References

1 Y. Shen and I. Dierking, *Appl. Sci.*, 2019, **9**, 2512–2559.
2 Y. Zhang, Q. Liu, H. Mundoor, Y. Yuan and I. I. Smalyukh, *ACS Nano*, 2015, **9**, 3097–3108.

3 J. Prakash, S. Khan, S. Chauhan and A. M. Biradar, *J. Mol. Liq.*, 2020, **297**, 112052.
4 A. Lorenz, N. Zimmermann, S. Kumar, D. R. Evans, G. Cook and H. Kitzerow, *Phys. Rev. E: Stat., Nonlinear, Soft Matter Phys.*, 2012, 051704.
5 P. Kopčanský, N. Tomašovičová, M. Koneracká, V. Závišová, M. Timko, A. Džarová, A. Šprincová, N. Iber, K. Fodor-Csorba, T. Tóth-Katona, A. Vajda and J. Jadzyn, *Phys. Rev. E: Stat., Nonlinear, Soft Matter Phys.*, 2008, **78**, 4–8.
6 Y. A. Garbovskiy and A. V. Glushchenko, Liquid crystalline colloids of nanoparticles: preparation, properties, and applications, *Solid State Phys.*, 2010, **62**, DOI: 10.1016/B978-0-12-374293-3.00001-8.
7 P. R. A. Keisham Nanao Singh, N. Monoranjan Singh and H. Basantakumar Sharma, *J. Adv. Phys.*, 2014, **8**, 2176–2188.
8 S. Mishra, V. Manjuladevi and R. Gupta, *J. Mol. Liq.*, 2023, **386**, 122482.
9 S. Orlandi, E. Benini, I. Miglioli, D. R. Evans and C. Zannoni, *Phys. Chem. Chem. Phys.*, 2016, **18**, 2428–2441.
10 S. Mishra, V. Manjuladevi and R. K. Gupta, *ACS Omega*, 2022, **7**, 46466–46474.
11 S. Mishra, M. V and R. Gupta, *Opt. Mater.*, 2023, **145**, 114392.
12 S. Mishra, A. M. Sontakke, R. K. Gupta, S. Kumar and V. Manjuladevi, *Mater. Today: Proc.*, 2021, **50**, 2587–2591.
13 S. Mishra, V. Manjuladevi, R. K. Gupta and S. Kumar, *Liq. Cryst.*, 2020, 1–11.
14 X. Yan, W. Liu, Y. Zhou, D. Yuan, X. Hu, W. Zhao and G. Zhou, *Appl. Sci.*, 2019, **9**, 1–11.
15 S. S J, S. Mishra, K. Dutta, R. K. Gupta and M. V, *J. Mol. Liq.*, 2022, **349**, 118168.
16 J. Kumar, V. Manjuladevi, R. K. Gupta and S. Kumar, *Liq. Cryst.*, 2016, **43**, 488–496.
17 J. Kumar, V. Manjuladevi, R. K. Gupta and S. Kumar, *Liq. Cryst.*, 2015, **42**, 361–369.
18 C. F. Hayes, *Mol. Cryst. Liq. Cryst.*, 1976, **36**, 245–253.
19 M. A. Bates, *J. Chem. Phys.*, 1999, **110**, 6553–6559.
20 R. Basu, L. J. Atwood and G. W. Sterling, *Crystals*, 2020, **10**(2), 123.
21 F. Ostovari and Z. Dehghani, *J. Mol. Liq.*, 2023, **375**, 121337.
22 M. Khodaee, N. Dalir, F. Feghhi, N. Ansari, M. Mohammadimasoudi, A. Goudarzi, A. F. Nasiri, M. Kolahdouz and S. Mohseni, *Sci. Rep.*, 2023, **13**, 1–11.
23 S. Al-Zangana, M. Iliut, M. Turner, A. Vijayaraghavan and I. Dierking, *Adv. Opt. Mater.*, 2016, **4**, 1541–1548.
24 M. Sahai, S. S. J, S. Kumar, R. K. Gupta and V. Manjuladevi, *Liq. Cryst.*, 2024, **51**(4), 543–557.
25 B. S. Witkowski, *Acta Phys. Pol., A*, 2018, **134**, 1226–1246.
26 M. D. McCluskey and S. J. Jokela, *J. Appl. Phys.*, 2009, **106**, 071101.
27 S. Sridevi, S. K. Prasad, G. G. Nair, V. D. Britto, B. L. V Prasad, S. Sridevi, S. K. Prasad, G. G. Nair, V. D. Britto and B. L. V Prasad, *Appl. Phys. Lett.*, 2015, **97**, 151913–151918.
28 H. Gruler, *Z. Naturforsch., A: Phys. Sci.*, 1975, **30**, 230–234.
29 H. Gruler, *Z. Naturforsch.*, 1972, **28a**, 765–770.